Ti^{3+} doped anodic single-wall TiO_2 nanotubes as highly efficient photocatalyst

Martin Motola[1,2], Mária Čaplovičová[3], Miloš Krbal[1], Hanna Sopha[1,4,&], Guru Karthikeyan Thirunavukkarasu[2], Maroš Gregor[5], Gustav Plesch[2], Jan M. Macak[1,4, &*]

[1]*Center of Materials and Nanotechnologies, Faculty of Chemical Technology, University of Pardubice, Nam.Čs.Legii 565, 530 02 Pardubice, Czech Republic*

[2]*Comenius University in Bratislava, Faculty of Natural Sciences, Department of Inorganic Chemistry, 842 15 Bratislava, Slovakia*

[3]*STU Centre for Nanodiagnostics, University Science Park Bratislava Centre, Slovak University of Technology, Vazovova 5, 812 43 Bratislava, Slovakia*

[4]*Central European Institute of Technology, Brno University of Technology, Purkynova 123, 612 00 Brno, Czech Republic*

[5]*Comenius University in Bratislava, Faculty of Mathematics Physics and Informatics, Department of Experimental Physics, 842 48 Bratislava, Slovakia*

[*]Corresponding author: e-mail address: jan.macak@upce.cz

[&] ISE Member

Abstract

In this work, a two-step treatment of TiO_2 nanotube (TNT) layers towards enhanced photocatalytic performance is presented. TNT layers with a thickness of ~7 μm and an average inner diameter of ~190 nm were prepared via electrochemical anodization of Ti foil in a fluoride containing ethylene glycol-based electrolyte. To improve the photocatalytic activity of the produced TNT layers a two-step post-treatment was conducted. First, the inner shell of the native double-wall TNT layers was removed via a mild pre-annealing followed by a selective etching treatment of the inner shell in piranha solution yielding single-wall TNT layers. Second, reduction via annealing in H_2/Ar atmosphere was performed. The resulting Ti^{3+} doped single-wall TNT layers possess 100% enhancement of photocatalytic activity compared to their non-treated counterparts.

Keywords: TiO_2 nanotube layers; single-wall; H_2 surface reduction; photoelectrochemistry; photocatalysis

1. Introduction

Since the pioneering work of Fujishima and Honda [1] in 1972 on the use of titanium dioxide (TiO_2) as a catalyst for the water splitting under UV light illumination, TiO_2 has gained great interests due to its exceptional physical and chemical properties. The mechanism of photocatalysis on TiO_2 surfaces is based on the UV light absorption, generation of e^-/h^+ pairs and subsequent formation of radicals with high oxidizing power [2,3]. Due to the relatively large band gap of ~3.2 eV for anatase TiO_2 a significant photoresponse can only be generated by UV irradiation. Therefore, it is crucial to improve the optical absorption and charge separation in order to enhance the photocatalytic activity.

So far, many approaches have been investigated to improve the photoactivity of TiO_2 including metal and non-metal doping or co-doping [4–13]. Among most recent and very promising approaches to improve the TiO_2 photocatalytic activity is the introduction of surface disorders within TiO_2 by hydrogenation [14–22]. Two phenomena are responsible for the photoactivity enhancement: 1) Newly created oxygen vacancies inhibit the recombination of charge carriers and therefore improve the photoactivity [20,22]; 2) Formation of defect states in the TiO_2 lattice by oxygen subtraction during the hydrogenation process, i.e. partial reduction of Ti^{4+} to Ti^{3+}. As a result, the Fermi level of the semiconductive TiO_2 is shifted towards its conduction band, which leads to a significant improvement of optical absorption and photoactivity [19,20,22]. Several techniques are available for the reduction of TiO_2: high- and low-pressure hydrogen thermal treatment, hydrogen plasma treatment, and (electro)-chemical reduction or oxidation [23].

The synthesis of self-organized TiO_2 nanotube (TNT) layers via electrochemical anodization of Ti foil was first reported in 1984 [24]. However, this unique one-dimensional (1D) nanomaterial has received a significant attention only after pioneering works [25,26] reported more than two decades later. TNT layers can be grown directly on the Ti surface by electrochemical

anodization in suitable aqueous- or organic-based electrolytes containing HF or fluoride salts [27–30]. Nowadays, ethylene glycol-based electrolytes containing NH_4F and H_2O are the most widely used electrolytes [31,32]. TNT layers are commonly accepted to be excellent materials in photoelectrochemical applications, in particular photocatalysis [33–38]. The exceptional geometry and electronic properties of TNT layers (such as high surface area, short diffusion path within enclosed nanoscale compartments) facilitate an effective charge transfer, a strong light absorption, and the ability to suppress the recombination of photogenerated e^-/h^+ pairs. These are also key advantages of the TNT layers which favor them compared to other TiO_2 nanostructures [39–43]. It is well-known that in common ethylene glycol-based electrolytes a double layer oxide structure is formed [44] composed of an inner and an outer shell, yielding the double-wall (DW) structure. The origin of DW can be explained considering the plastic flow model for the nanotube formation [45,46]. Recent papers studied the exact composition of the inner and outer shell [47,48]. The results show a high C and F contamination of the inner shell, originating from the voltage induced decomposition of the electrolyte while the outer shell consists of almost pure TiO_2. Several studies report that the removal of the inner shell has a positive impact on the efficiency of DSSCs [46,49–51]. Moreover, we recently reported on enhanced photoelectrochemical properties of such single-wall (SW) TNT layers [52]. To the best of our knowledge, there is no study on the photocatalytic performance of SW TNT layers.

Regarding the reduction of TNT layers by annealing in H_2/Ar atmosphere, an improved electrochemical performance as electrode materials for supercapacitors [53], an improved power density for lithium-ion batteries [54] and an enhanced photocatalytic activity [21,55,56] were already reported. So far, a two-step treatment combining the inner shell removal and the reduction of TNT layers and study of their photoelectrochemical and photocatalytic performance has not been reported yet.

Here, we present a combination of the inner shell removal and the reduction by a low-pressure annealing in H_2/Ar atmosphere to achieve a highly efficient photocatalyst based on SW anodic TNT layers. The influence of both treatments on photoelectrochemical performance and photocatalytic activity of such SW TNT layers is investigated and discussed.

2. Experimental

2.1 Synthesis of pristine and modified TNT layers

Titanium foil (Sigma-Aldrich, 2x1 cm with 0.127 mm thickness, 99.7% purity) was used as a starting substrate for the growth of TNT layers. The electrochemical anodization, conducted at 80 V for 4 h at room temperature in ethylene glycol-based (CentralChem, Slovakia) electrolyte containing 130 mM NH_4F (CentralChem, Slovakia) and 12 wt.% distilled H_2O, led to the synthesis of self-organized double-wall (DW) TNT layers. As previously reported, an etching treatment [52] was used to remove the C- and F-rich inner shell. First, as-prepared DW layers were pre-annealed in air at 150 °C for 1 h. Second, the DW layers were immersed in piranha solution for 8 min at 70°C. Finally, the etched TNT layers were immersed in H_2O and EtOH for 1 min, respectively, and dried with a nitrogen stream, yielding SW TNT layers. In order to obtain anatase structure, both types of TNT layers were annealed in a muffle oven at 450 °C for 2h [21]. Non-reduced TNT layers were annealed in air while to obtain reduced SW and DW TNT layers, annealing in 5% H_2/Ar at 450 °C for 2 h was additionally conducted, yielding r-SW and r-DW, respectively. XRD patterns of all types of TNT layers are reported in Supplementary file (Fig. S1).

2.2 Material characterization

The crystal structure of TNT layers was characterized by X-ray Diffractometer (XRD, PANalytical, Cu Kα radiation, λ = 1.5418 Å) in the grazing incidence mode. To evaluate the partial reduction of Ti^{4+} to Ti^{3+} and Fermi levels, X-ray Photoelectron Spectroscopy (XPS,

Omicron multi-probe system) with hemispherical analyzer (monochromatic Al K-alpha X-rays 1486.6 eV) was performed. The overall morphology of the TNT layers was investigated by Scanning Electron Microscope (SEM, Lyra 3 Tescan, at 10 and 30 kV). The morphology of individual nanotubes and nanotube walls was characterized by analytical Transmission Electron Microscope with atomic resolution (JEM ARM 200 cF, JEOL, at 200 kV). For the Energy Dispersive X-ray Spectroscopy (EDX) a large angle detector (JEOL JED-2300T CENTURIO SDD) with solid angle up to 0.98 sr and a detection area of 100 mm^2 was used. For the Electron Energy Loss Spectroscopy (EELS) measurements post column GIF Quantum ER spectrometer with DualEELS capability was employed. The samples were prepared by scratching the nanotubes on a carbon-coated copper grid.

2.3 Photoelectrochemical and photocatalytic activity measurements

The photocurrent measurements of TNT layers were carried out in aqueous solution 0.1 M Na_2SO_4 at 0.4 $V_{vs.Ag/AgCl}$ in the spectral range from 300 to 450 nm. A photoelectric spectrophotometer (Instytut Fotonowy) with a 150 W Xe lamp and a monochromator with a bandwidth of 10 nm connected with a modular electrochemical system AUTOLAB (PGSTAT 204; MetrohmAutolab B. V.; Nova 1.10 software) was used for the photocurrent measurements. Photocurrent stability tests were carried out by measuring the photocurrent produced under chopped light irradiation (light/dark cycles of 10s). Cyclic voltammograms were recorded in the potential range from -0.4 V to 1 V vs. 3 M Ag/AgCl with a sweep rate of 5 mV/s, starting at 0 V towards positive voltages in the dark and at 350 nm, respectively.

The photocatalytic activity was investigated by monitoring the photodegradation of methylene blue (MB) and rhodamine B (RB) solutions with an initial concentrations of 10^{-5} mol/L under constant bubbling with air in a self-constructed apparatus [4] using a polychromatic light irradiation (mercury lamp HPA 400 W, Philips, wavelength range 300 – 800 nm; λ_{MAX}= 365 nm, 6.51 mW/cm^2). Prior to each measurement, a sample was placed for 60 min in the dye

solution in the dark to achieve an adsorption/desorption equilibrium. The decrease in the dye concentration was estimated from the absorbance of the solution measured at 553 nm for RB and at 670 nm for MB using an UV-VIS spectrophotometer (Jasco V-530). In addition, we conducted photocatalytic experiments with aqueous phenol solution using Total Organic Carbon (TOC) analysis. The description of these experiments is extensive and it is provided in the Supplementary file. To investigate the stability of the samples, the photocatalytic measurements were performed 3 times (with 1-week step). Generally, the differences between repeated measurements did not exceed ±5%.

3. Results and discussion

3.1 Morphology, structure, and composition of TNT layers

Fig. 1A and B show representative top-view and cross-sectional SEM images of self-organized TNT layers with a thickness of ~7 μm and an average inner tube diameter of ~190 nm. Due to the nature of nanotube formation in ethylene glycol based electrolytes [44], the presence of the inner shell at the bottom parts of the TNT layers is revealed and is clearly visible by SEM as the porous areas within the interiors of nanotubes (Fig. 1C). Fig. 1D shows the TNT layers after complete removal of the inner shell and single-wall morphology with no visible porous areas within the nanotubes were observed. To point out, prolonging the etching time and/or increasing the temperature during etching over the optimized values results in the TNT layers to peel off from the Ti substrate. For shorter time and/or lower temperatures, the inner shell is not completely dissolved.

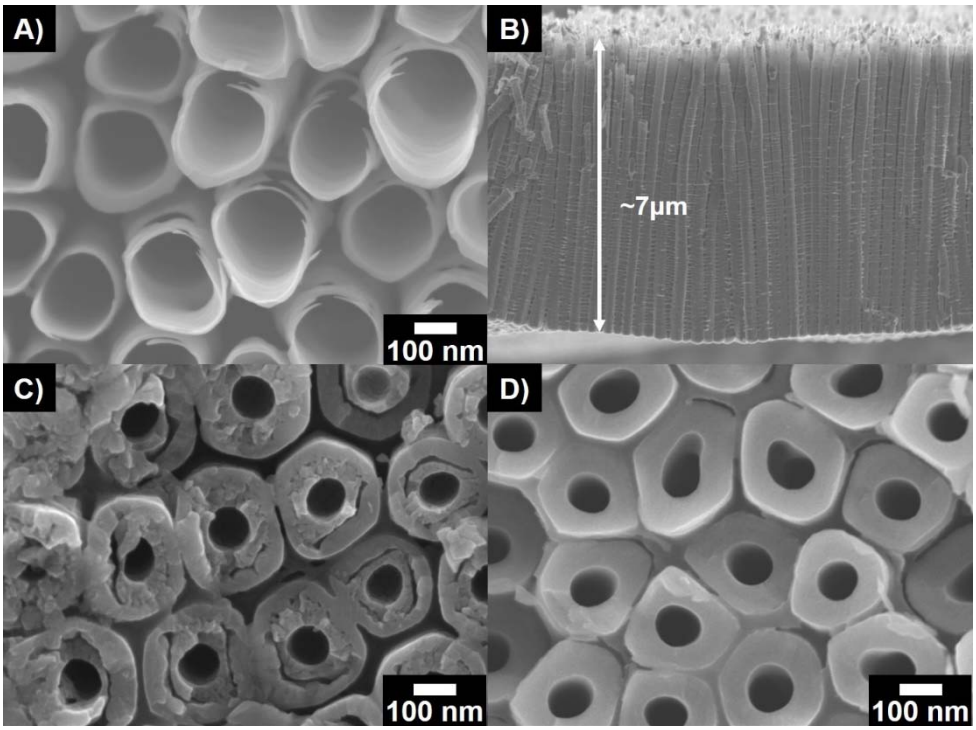

Fig. 1. SEM images of TiO_2 nanotube layers: (A) top-view, (B) cross-sectional view, (C) double-wall structure and (D) single-wall structure of the nanotube bottoms, respectively.

To obtain additional information on the morphology, crystalline structure and composition of TNT layers, TEM-related techniques (Fig. 2, Fig. S2) and XPS (Fig. 3) analyses were carried out.

Fig. 2A shows a representative top-view image of DW TNT layers obtained from the bottom part of the layer. The total thickness of the inner shell is ~60 nm. EDX analysis determined 17.8 at % of C and 9.5 at % of F. EDX mapping identified that F is mainly situated on the outer wall of the nanotube while carbon is predominantly localized within the nanotube. These observations are in good agreement with the literature [47,48]. Fig. 2B shows a detailed side-view HAADF STEM image of the DW nanotube fragment after annealing in air. The compact outer and the porous inner shell can be clearly distinguished. The inner shell composition did not significantly change neither upon annealing at 450 °C in air nor after reduction in H_2/Ar atmosphere (17.2 at % of C and 9.7 at % of F). Using SAED (Fig. 2C) solely anatase phase was

identified in the case of all TNT layers annealed at 450 °C. Straight lattice fringes with a spacing of 0.35 nm, depicted by BF STEM mode from the outer wall of the nanotube (Fig. 2D), were assigned to the (101) plane of anatase. The outer wall of the nanotube is well crystalline with no visible crystal defects and/or amorphous content. The nanotube wall is viewed along <010> direction, as follows from the relevant Fast Fourier Transform.

Point by point EELS analyzes across the nanotube wall of the reduced SW were carried out to investigate the differences in the local chemical composition close to the surface and in the bulk (Fig S2). Overall 19-point analyses were conducted and recorded by Dual EELS method at identical conditions. Some of them (measurements 9, 10, 11, 12, 13, and 16) are highlighted in the inset of Fig. S2. Close to the nanotube wall surface, the Ti-$L_{2,3}$ edge is shifted to a lower energy by 1.5 eV. The energy loss of Ti-$L_{2,3}$ position edges is sensitive to the valence of Ti and the shift of Ti-$L_{2,3}$ edge to lower energy region indicates the valence reduction of Ti^{4+} to Ti^{3+} which is accompanied by a loss of O from the surface of anatase TiO_2 [57]. According to our measurements, the lowered valence state Ti^{3+} was identified close to the surface up to 3 nm in depth (up to point 9 in Fig. S2). As for the data obtained from the body of nanotube wall over depth of 3 nm, solely the presence of Ti^{4+} was confirmed. Obtained EELS data clearly indicate the partial surface reduction of Ti^{4+} to Ti^{3+} during annealing in H_2/Ar atmosphere.

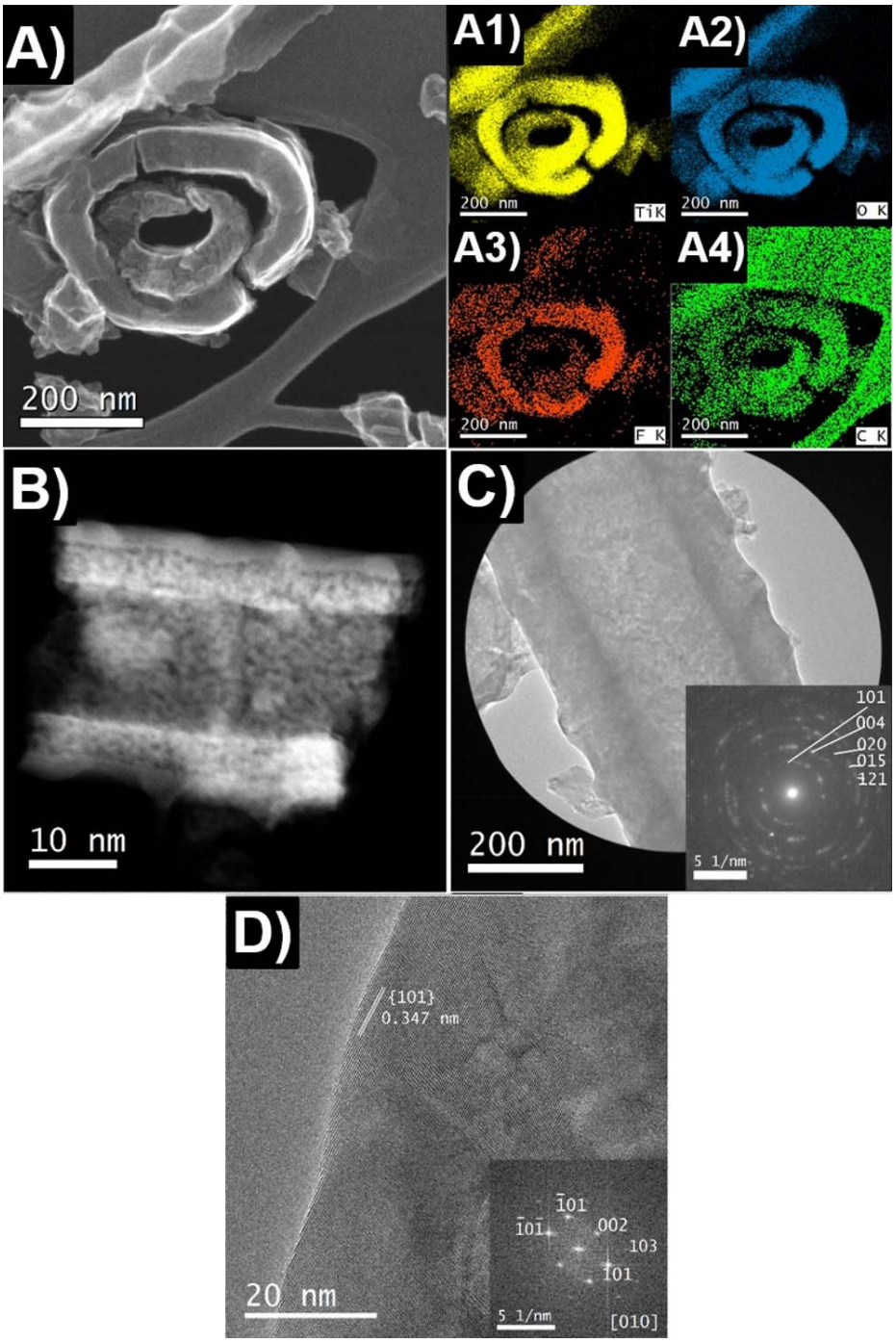

Fig. 2. (A) TEM image of double-wall morphology of a nanotube (taken at the bottom part of the TNT layer), two broken separated walls are depicted. EDX mapping of Ti (A1), O (A2), F (A3), and C (A4); (B) HAADF STEM image of a fragment of double-wall nanotube annealed in air; (C) TEM and corresponding SAED image of double-wall nanotube, anatase reflection are assigned to individual SAED rings; (D) HRTEM image of outer nanotube wall with relevant FFT pattern (as an inset) indicating single crystalline nature of the wall.

Finally, the chemical binding within TNT layers was analyzed by XPS. Figure 3 shows high-resolution scans of Ti2p state, O1s state and valence band maxima (VBM) position. All TNT layers show the presence of Ti^{4+} – O bond in the Ti2p spectrum (Fig. 3A), with binding energy of ~458.7 eV and ~464.5 eV corresponding to Ti $2p_{3/2}$ and Ti $2p_{1/2}$, respectively. The reduced Ti^{3+} peak with binding energy of ~457 eV is not clearly visible, due to the rapid oxidation of the surface in the ambient atmosphere [22]. The oxygen spectrum in Fig. 3B shows asymmetrical O1s peak for all TNT layers, deconvoluted after a Shirley background subtraction, using mixed Gauss-Lorentz function (GL30) into two peaks centered at ~530 eV and ~531.3 eV, and can be attributed to TiO_2 and Ti-O-H and/or C=O bonds, respectively. Finally, the VBM of TNT layers were estimated from XPS spectra by a linear extrapolation of the peaks with the baseline near a Fermi energy (Fig. 3C). A small negative shift of valance band maxima around 0.2 eV was observed for reduced TNT layers. This band gap narrowing, observed after reduction of the TNT layers, is attributed to the formation of localized Ti^{3+} states. In the Ti^{3+} doped TNT layers, the newly created oxygen vacancies form donor levels in below the conduction band of TiO_2. These defects act as important adsorptive and active sites for heterogeneous catalysis thus enhance the light absorption and electronic conductivity of TNT layers [19].

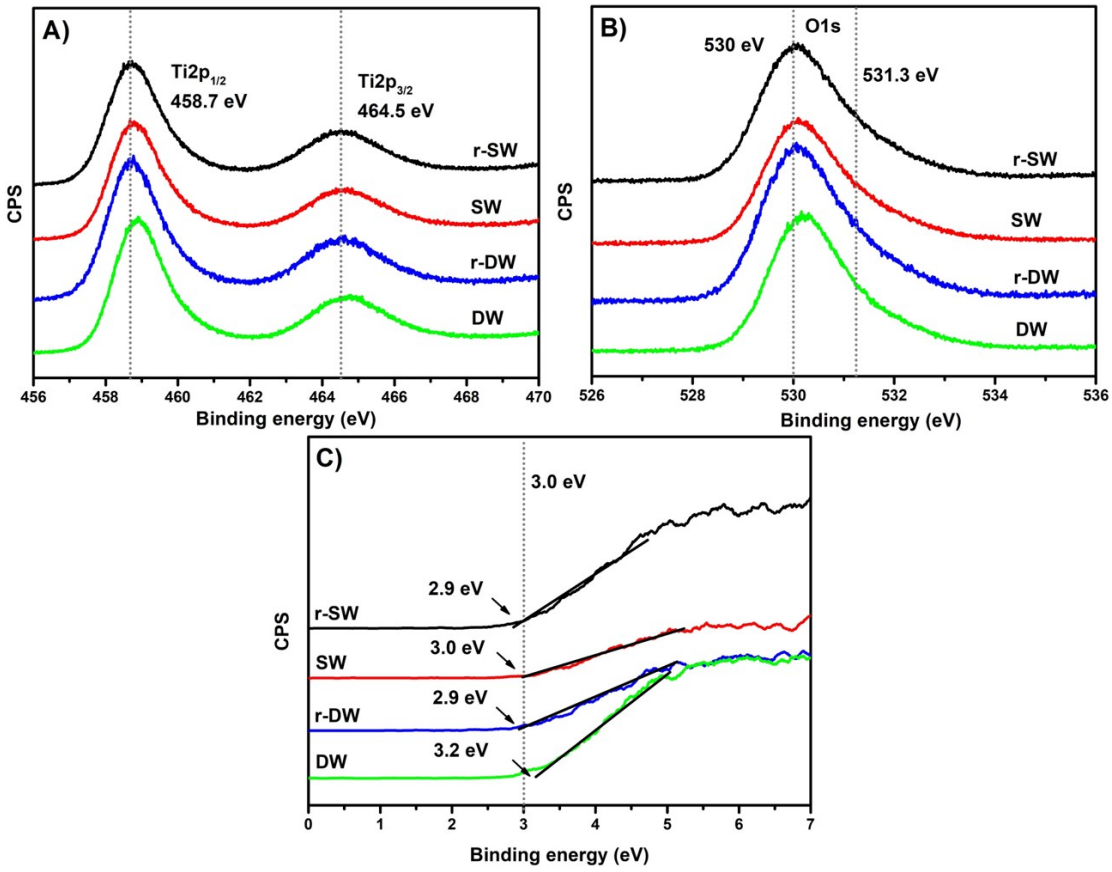

Fig. 3. XPS spectra showing (A) Ti2p peak, (B) O1s deconvoluted peak and (C) valence band maxima (VBM), respectively, of single-wall (SW), reduced single-wall (r-SW), double-wall (DW) and reduced double-wall (r-DW) TiO_2 nanotube layers.

3.2 Photoelectrochemical and photocatalytic performance of TNT layers

Fig. 4A shows the incident photon-to-electron conversion efficiencies (IPCE) in the wavelength range from 300 to 450 nm. The IPCE data are in agreement with the obtained photocurrent densities (Fig. S3). The ~5% increase in IPCEs for both SW TNT layers compared to DW ones in the range from ~325 nm to ~375 nm is ascribed to the removal of the inner shell which enhances the incident light absorption [52]. For further analysis, photocurrent transients were recorded and examined in detail. As the I_{MAX} of the used light irradiation source for photocatalysis is at the wavelength of 365 nm, the photocurrent transients at 350 nm, 360 nm,

370 nm, and 380 nm are presented in Fig. 4B. The photocurrent transients from 300 nm to 500 nm are shown in the Supplementary information (Fig. S3).

Fig. 4C and D shows cyclic voltammetry (CV) curves obtained in the dark and under UV irradiation (λ = 350 nm), respectively. In general, the CV shape for all TNTs is typical for the anatase structure [45]. The dark currents are almost identical for all TNTs. After UV irradiation, the photocurrent densities are comparable for all TNTs. The photocurrent densities for all TNTs increased until the potential of ~0.4 V. At higher potentials a photocurrent plateau was observed indicating that the thickness of the nanotube walls equals the space charge layer [58]. For SW and r-SW, the photocurrents are higher than for DW and r-DW, however, the difference is not pronounced. Based on the obtained photoelectrochemical results (Fig.4A-C), the reduction in H_2/Ar atmosphere had little or no effect on the photoelectrochemical performance of TNT layers.

All TNT layers were explored for the photocatalytic degradation of MB and RB under UV light irradiation. Fig. 4E and F shows the corresponding decomposition rates of MB and RB, respectively. For both dyes, the highest decomposition rates were obtained using r-SW TNT layers. The photocatalytic degradation of organic dyes follows the first-order reaction [37]:

$$\ln (c/c_0) = - kt \quad (1)$$

where c_0 and c are the initial and after the time t concentrations, respectively, and k is the pseudo-first-rate kinetic constant.

The obtained photocatalytic results indicate that both employed modifications (i.e. removal of the inner shell and the reduction in H_2/Ar atmosphere) increase the photodegradation rate of MB and RB under UV light irradiation. When one compares these modifications, the reduction by annealing leads to more distinct improvement of the photoactivity than the inner shell removal. Indeed, the presence of Ti^{3+} in reduced TNT layers contributes to an improved charge

carriers transfer efficiency and limits the e^-/h^+ pair recombination by introducing intra-band gap states in anatase TiO_2 [59]. On the other hand, the distinct porous morphology of the inner shell in DW and r-DW (visible in Fig. 1C) have a negative contribution to the charge recombination [46]. Therefore, the photocatalytic activity follows trends of SW being better than DW and r-SW being better than r-DW. Overall, the photodegradation rate of r-SW ($k = 0.029\ min^{-1}$ for MB; $k = 0.028\ min^{-1}$ for RB) is enhanced by ~100% compared to the DW ($k = 0.014\ min^{-1}$ for MB; $k = 0.014\ min^{-1}$ for RB), by ~50% compared to the SW ($k = 0.019\ min^{-1}$ for MB; $k = 0.017\ min^{-1}$ for RB) and by ~20% compared to the r-DW ($k = 0.023\ min^{-1}$ for MB; $k = 0.023\ min^{-1}$ for RB).

To further prove that TNT layers are responsible for the enhanced photocatalytic activity and to exclude the possible degradation of MB and RB via dye-sensitization and/or reduction [60,61], additional photocatalytic tests were carried out with an aqueous phenol solution, using TOC analysis. The results are shown in Figure S4 in the Supplementary file. Nevertheless, a similar trend where the photocatalytic activity follows the order r-SW>r-DW>SW>DW (where r-SW is the most active photocatalyst) was obtained. The phenol solution was fully degraded after 150 min using r-SW. This clearly proves the efficient degradation of studied pollutants as a result of a photocatalytic reaction on the solid/liquid interface between TNT layers/organic pollutant. The possible dye-sensitization and/or reduction in case of MB and RB can therefore be refuted.

Table 1. Summary of 1D Ti^{3+} doped TiO_2 photocatalysts under UV light irradiation. The rate constants and removal efficiencies were directly taken from the cited references, wherever possible.

Photocatalyst	**Weight**	**Irradiation (λ_{MAX})**	**Target pollutant & concentration**	**Time**	**Removal efficiency**	**Rate constant**	**Ref.**
N-Ti^{3+}- TiO_2 nanotubes	-	N/A	Diclofenac (5 mg/L)	4h	100%	N/A	[62]

N-Ti^{3+}- TiO_2 nanorods	-	365 nm	2-ME (N/A)	-	31%	N/A	[63]
			BE (N/A)		37%	N/A	
			2-ATP (N/A)		42%	N/A	
N-Ti^{3+}-TiO_2 nanorods	20 mg	N/A	MB (10 mg/L)	120 min	88%	N/A	[64]
Ti^{3+}-TiO_2/g-C_3N_4 nanotubes	40 mg	450 nm	MB (20 mg/L)	100 min	100%	0.038 min^{-1}	[65]
Ti^{3+}-TiO_2 nanotubes	10 mg	365 nm	RB (10^{-6} mol/L)	100 min	60%	0.018 min^{-1}	[21]
Ag/S-Ti^{3+}-TiO_2	25 mg	N/A	Phenol (10mg/L)	180min	99%	0.029 min^{-1}	[66]
This work	<10 mg	365 nm	MB (10^{-5} mol/L)	100 min	100%	0.029 min^{-1}	-
			RB (10^{-5} mol/L)	100 min	100%	0.028 min^{-1}	
			Phenol (10mg/L)	150 min	99%	N/A	

In Table 1, the photocatalytic activity of our most efficient r-SW is compared to other reports on 1D Ti^{3+} doped TiO_2 photocatalysts found in literature. Considering the fact that the amount of TNTs on the area of 2 cm^2 (area with nanotubes used for photocatalytic degradation) is less than 10 mg, the photocatalytic efficiency of r-SW is enhanced compared to previous reports where the amount of photocatalyst is 2.5 - 4 times higher (25 - 40 mg) [21,62–67].

The observed photocatalytic trend is not fully in the agreement with photocurrent results; however, the difference can be described as follows. The photodegradation of the dye solutions proceeds on the liquid/solid interfaces. The low-pressure hydrogenation of the surface of anatase TiO_2 leads to the creation of Ti centers or unpaired electrons, and subsequently forms donor levels in the electronic structure of TiO_2 [18]. Oxygen vacancies suppress the recombination of photogenerated e^-/h^+ which consequently improve the photocatalytic activity. Moreover, the oxygen vacancies act as e^- donors, increasing the donor density in reduced TiO_2 [18]. The increased donor density results in an increased charge transport and shifts the Fermi level of TiO_2 towards the conduction band. Contrary, when the photocurrent is collected, the

photogenerated e^- have to be transported to the positive electrode across the whole thickness of TNT layers. Due to this fact, the Ti^{3+} and oxygen vacancies are necessary in the whole bulk of the nanotube wall to efficiently trap the generated e^- thus improve the photocurrent density. The effect of the surface/bulk defects on the photocatalytic activity of TiO_2 was previously reported [68]. In general, the photogenerated e^- on the surface of TiO_2 can reduce electron acceptors and the photogenerated h^+ can oxidize electron donors, initiating the photo-redox reaction. However, considering the fact that only surface defects are present in r-DW and r-SW, the photogenerated h^+ can be trapped in the bulk through electrostatic interaction [68]. The trapped h^+ in the bulk are not available in the photocatalytic reaction anymore and they rather act as new recombination centers. On the other hand, the photogenerated h^+ can also be trapped by surface defects (i.e. defects clusters) and the separation of e^-/h^+ pairs is facilitated. These defects clusters are ready to react with electron donors and the photocatalytic reaction is greatly promoted while the photoelectrochemical performance is not affected significantly. In order to obtain simultaneous enhancement of photocatalytic and photoelectrochemical performance of TiO_2, both surface and bulk defects are necessary. All in all, the presence of surface defects plays a vital role in the enhancement of the photocatalytic activity with little or no effect on the photoelectrochemical performance of TNT layers.

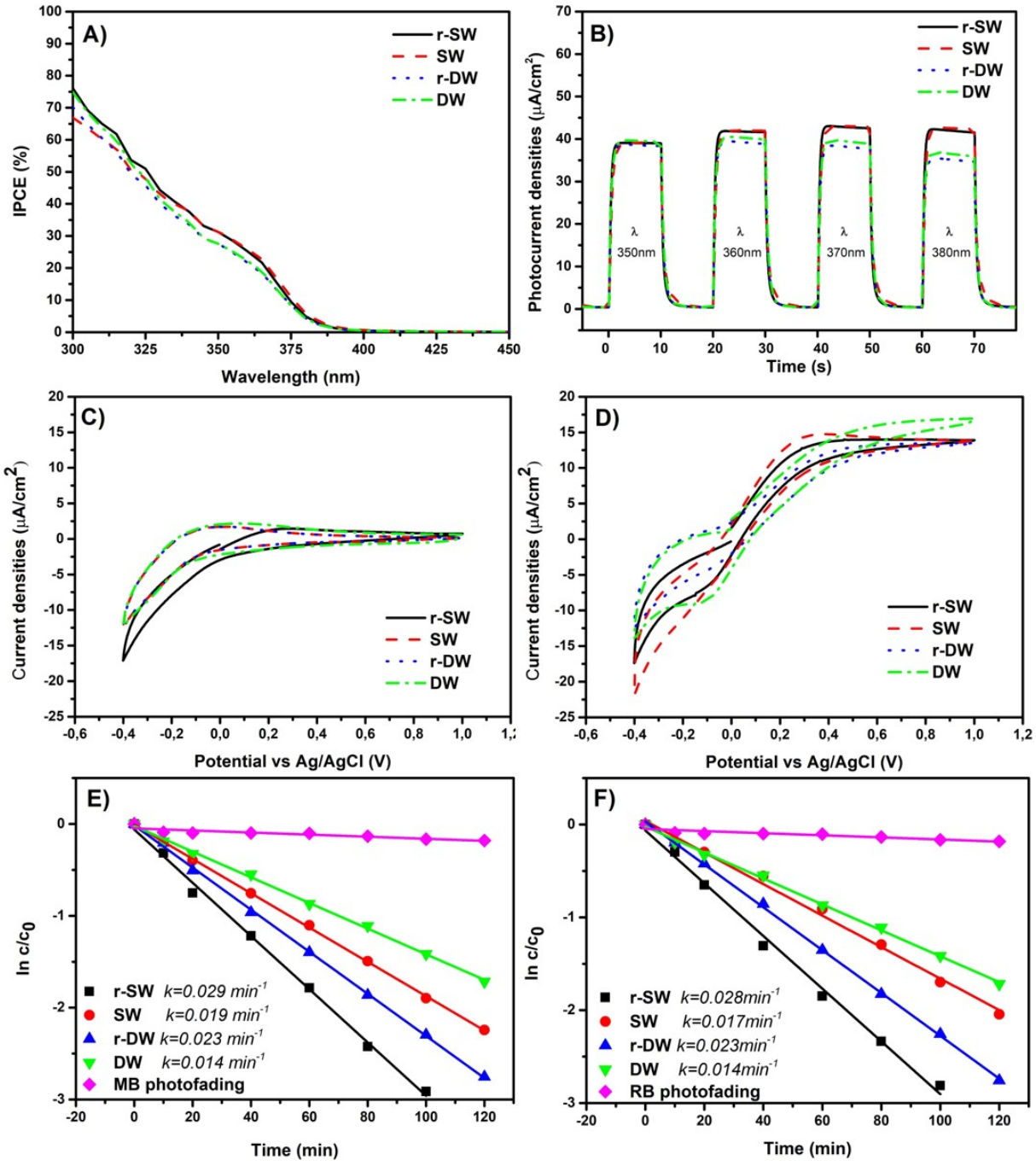

Fig. 4. (A) Incident photon-to-electron conversion efficiencies (IPCE) vs wavelength, (B) photocurrent transients recorded at 350 nm, 360 nm, 370nm, and 380 nm, respectively, CV curves (C) in the dark, (D) under UV irradiation (λ = 350 nm) and photocatalytic decomposition rates of (E) methylene blue (MB) and (F) rhodamine B (RB) for single-wall (SW), reduced single-wall (r-SW), double-wall (DW) and reduced double-wall (r-DW) TiO_2 nanotube layers.

4. Conclusions

In this work, we present a two-step treatment of TNT layers to enhance their photocatalytic performance. Optimized etching treatment in piranha solution led to the dissolution of C and F containing inner shell and the consequent formation of SW TNTs. Low-pressure annealing in H_2/Ar led to partial surface reduction of Ti^{4+} to Ti^{3+}. The combination of these two treatments results in an enhanced photocatalytic performance in degradation of organic dyes and phenol compared to the non-treated, solely hydrogenated, or solely etched counterparts due to an improved transfer efficiency of charge carriers and decelerating the e^-/h^+ recombination rate. Such two-step treated TNT layers possess 100% and more than 20% enhancement in photocatalytic activity compared to the non-treated and single-step treated TNT layers, respectively.

Acknowledgements

The authors acknowledge the financial support from the European Research Council (ERC No. 638857) and the Ministry of Education, Youth and Sports of the Czech Republic (projects LM2015082, LQ1601). This publication is the result of the project implementation: Independent research and development of new super-hard coatings and their characterization by advanced experimental techniques - NEOCOATINGS, NFP313010T598, supported by the ESIF. Operational Program Research and Development ITMS:26210120010 along with the Scientific Grant Agency of the Slovak Republic (project VEGA 1/0712/18) and Slovak Research and Development Agency (project APVV-17-0324) have also supported this research. Mr. Ludek Hromadko is acknowledged for the SEM investigation.

References

[1] A. Fujishima, K. Honda, Electrochemical photolysis of water at a semiconductor electrode., Nature. 238 (1972) 37–8. http://www.ncbi.nlm.nih.gov/pubmed/12635268 (accessed March 3, 2019).

[2] T.L.T. and, J.. John T. Yates, Surface Science Studies of the Photoactivation of TiO2New Photochemical Processes, (2006). doi:10.1021/CR050172K.

[3] J. Schneider, M. Matsuoka, M. Takeuchi, J. Zhang, Y. Horiuchi, M. Anpo, D.W. Bahnemann, Understanding TiO 2 Photocatalysis: Mechanisms and Materials, Chem. Rev. 114 (2014) 9919–9986. doi:10.1021/cr5001892.

[4] R. Michal, E. Dworniczek, M. Čaplovičová, M. Gregor, L. Čaplovič, A. Seniuk, P. Kuš, G. Plesch, Photocatalytic and photodisinfectant activity of sulfated and Eu doped anatase against clinically important microorganisms, Ceram. Int. 40 (2014) 5745–5756. doi:10.1016/J.CERAMINT.2013.11.013.

[5] G. Williams, B. Seger, P. V. Kamat, TiO 2 -Graphene Nanocomposites. UV-Assisted Photocatalytic Reduction of Graphene Oxide, ACS Nano. 2 (2008) 1487–1491. doi:10.1021/nn800251f.

[6] M. Anpo, S. Dohshi, M. Kitano, Y. Hu, M. Takeuchi, M. Matsuoka, The Preparation and characterization of highly efficient titanium oxide-based photofunctional materials, Annu. Rev. Mater. Res. 35 (2005) 1–27. doi:10.1146/annurev.matsci.35.100303.121340.

[7] T. Ohno, F. Tanigawa, K. Fujihara, S. Izumi, M. Matsumura, Photocatalytic oxidation of water by visible light using ruthenium-doped titanium dioxide powder, J.

Photochem. Photobiol. A Chem. 127 (1999) 107–110. doi:10.1016/S1010-6030(99)00128-8.

[8] C. Burda, Y. Lou, X. Chen, A.C.S. Samia, A. John Stout, J.L. Gole, Enhanced Nitrogen Doping in TiO2 Nanoparticles, Nano Lett. 3 (2003) 1049–1051. doi:10.1021/NL034332O.

[9] L. Lin, W. Lin, Y. Zhu, B. Zhao, Y. Xie, Phosphor-doped Titania —a Novel Photocatalyst Active in Visible Light, Chem. Lett. 34 (2005) 284–285. doi:10.1246/cl.2005.284.

[10] S. Sakthivel, H. Kisch, Daylight Photocatalysis by Carbon-Modified Titanium Dioxide, Angew. Chemie Int. Ed. 42 (2003) 4908–4911. doi:10.1002/anie.200351577.

[11] F. Dong, W. Zhao, Z. Wu, Characterization and photocatalytic activities of C, N and S co-doped TiO 2 with 1D nanostructure prepared by the nano-confinement effect, Nanotechnology. 19 (2008) 1–10. doi:10.1088/0957-4484/19/36/365607.

[12] J. Zhang, C. Pan, P. Fang, J. Wei, R. Xiong, Mo + C Codoped TiO_2 Using Thermal Oxidation for Enhancing Photocatalytic Activity, ACS Appl. Mater. Interfaces. 2 (2010) 1173–1176. doi:10.1021/am100011c.

[13] M. Xing, Y. Wu, J. Zhang, F. Chen, Effect of synergy on the visible light activity of B, N and Fe co-doped TiO2 for the degradation of MO, Nanoscale. 2 (2010) 1233–1239. doi:10.1039/c0nr00078g.

[14] X. Chen, L. Liu, P.Y. Yu, S.S. Mao, Increasing Solar Absorption for Photocatalysis with Black Hydrogenated Titanium Dioxide Nanocrystals, Science (80-.). 331 (2011) 746–750. doi:10.1126/science.1200448.

[15] W.H. Saputera, G. Mul, M.S. Hamdy, Ti3+-containing titania: Synthesis tactics and

photocatalytic performance, Catal. Today. 246 (2015) 60–66. doi:10.1016/j.cattod.2014.07.049.

[16] B. Sun, T. Shi, X. Tan, Z. Liu, Y. Wu, G. Liao, Titanium Dioxide Nanorods with Hydrogenated Oxygen Vacancies for Enhanced Solar Water Splitting, J. Nanosci. Nanotechnol. 16 (2016) 6148–6154. doi:10.1166/jnn.2016.11036.

[17] J. Ma, H. Wu, Y. Liu, H. He, Photocatalytic Removal of NO_x over Visible Light Responsive Oxygen-Deficient TiO_2, J. Phys. Chem. C. 118 (2014) 7434–7441. doi:10.1021/jp500116n.

[18] S. Bagheri, N. Muhd Julkapli, Synergistic effects on hydrogenated TiO2 for photodegradation of synthetic compounds pollutants, Int. J. Hydrogen Energy. 41 (2016) 14652–14664. doi:10.1016/J.IJHYDENE.2016.06.179.

[19] L. Chen, F. He, Y. Huang, Y. Meng, R. Guo, Hydrogenated nanoporous TiO2 film on Ti 25Nb 3Mo 2Sn 3Zr alloy with enhanced photocatalytic and sterilization activities driven by visible light, J. Alloys Compd. 678 (2016) 5–11. doi:10.1016/j.jallcom.2016.03.216.

[20] Y. Liu, L. Tian, X. Tan, X. Li, X. Chen, Synthesis, properties, and applications of black titanium dioxide nanomaterials, Sci. Bull. 62 (2017) 431–441. doi:10.1016/j.scib.2017.01.034.

[21] M. Motola, L. Satrapinskyy, M. Čaplovicová, T. Roch, M. Gregor, B. Grančič, J. Greguš, Ľ. Čaplovič, G. Plesch, Enhanced photocatalytic activity of hydrogenated and vanadium doped TiO<inf>2</inf>nanotube arrays grown by anodization of sputtered Ti layers, Appl. Surf. Sci. 434 (2018). doi:10.1016/j.apsusc.2017.11.253.

[22] E.M. Samsudin, S. Bee, A. Hamid, J.C. Juan, W. Jefrey Basirun, A.E. Kandjani,

Surface modification of mixed-phase hydrogenated TiO 2 and corresponding photocatalytic response, Appl. Surf. Sci. 359 (2015) 883–896. doi:10.1016/j.apsusc.2015.10.194.

[23] X. Chen, L. Liu, F. Huang, Black titanium dioxide (TiO 2) nanomaterials, Chem. Soc. Rev. 44 (2015) 1861–1885. doi:10.1039/C4CS00330F.

[24] M. Assefpour-Dezfuly, C. Vlachos, E.H. Andrews, Oxide morphology and adhesive bonding on titanium surfaces, J. Mater. Sci. 19 (1984) 3626–3639. doi:10.1007/BF02396935.

[25] J.M. Macak, H. Tsuchiya, A. Ghicov, K. Yasuda, R. Hahn, S. Bauer, P. Schmuki, TiO2 nanotubes: Self-organized electrochemical formation, properties and applications, Curr. Opin. Solid State Mater. Sci. 11 (2007) 3–18. doi:10.1016/J.COSSMS.2007.08.004.

[26] S.P. Albu, A. Ghicov, J.M. Macak, P. Schmuki, 250 μm long anodic TiO2 nanotubes with hexagonal self-ordering, Phys. Status Solidi – Rapid Res. Lett. 1 (2007) R65–R67. doi:10.1002/pssr.200600069.

[27] J.M. Macak, K. Sirotna, P. Schmuki, Self-organized porous titanium oxide prepared in Na2SO4/NaF electrolytes, Electrochim. Acta. 50 (2005) 3679–3684. doi:10.1016/J.ELECTACTA.2005.01.014.

[28] Kai Zhu, Nathan R. Neale, and Alexander Miedaner, A.J. Frank*, Enhanced Charge-Collection Efficiencies and Light Scattering in Dye-Sensitized Solar Cells Using Oriented TiO2 Nanotubes Arrays, (2006). doi:10.1021/NL062000O.

[29] J.M. Macak, H. Tsuchiya, L. Taveira, S. Aldabergerova, P. Schmuki, Smooth Anodic TiO2 Nanotubes, Angew. Chemie Int. Ed. 44 (2005) 7463–7465. doi:10.1002/anie.200502781.

[30] J.M. Macak, H. Tsuchiya, A. Ghicov, K. Yasuda, R. Hahn, S. Bauer, P. Schmuki, TiO2 nanotubes: Self-organized electrochemical formation, properties and applications, Curr. Opin. Solid State Mater. Sci. 11 (2007) 3–18. doi:10.1016/J.COSSMS.2007.08.004.

[31] K. Lee, A. Mazare, P. Schmuki, One-Dimensional Titanium Dioxide Nanomaterials: Nanotubes, Chem. Rev. 114 (2014) 9385–9454. doi:10.1021/cr500061m.

[32] H. Sopha, L. Hromadko, K. Nechvilova, J.M. Macak, Effect of electrolyte age and potential changes on the morphology of TiO2 nanotubes, J. Electroanal. Chem. 759 (2015) 122–128. doi:10.1016/J.JELECHEM.2015.11.002.

[33] N.R. de Tacconi, C. R. Chenthamarakshan, G. Yogeeswaran, A. Watcharenwong, R. S. de Zoysa, N.A. Basit, K. Rajeshwar, Nanoporous TiO2 and WO3 Films by Anodization of Titanium and Tungsten Substrates: Influence of Process Variables on Morphology and Photoelectrochemical Response†, J Phys. Chem. BPhys. Chem. B. 110 (2006) 25347–25355. doi:10.1021/JP064527V.

[34] H. Sopha, M. Krbal, S. Ng, J. Prikryl, R. Zazpe, F.K. Yam, J.M. Macak, Highly efficient photoelectrochemical and photocatalytic anodic TiO2 nanotube layers with additional TiO2 coating, Appl. Mater. Today. 9 (2017) 104–110. doi:10.1016/J.APMT.2017.06.002.

[35] M. Motola, L. Satrapinskyy, T. Roch, J. Šubrt, J. Kupčík, M. Klementová, M. Jakubičková, F. Peterka, G. Plesch, Anatase TiO<inf>2</inf>nanotube arrays and titania films on titanium mesh for photocatalytic NO<inf>X</inf>removal and water cleaning, Catal. Today. 287 (2017). doi:10.1016/j.cattod.2016.10.011.

[36] I. Paramasivam, H. Jha, N. Liu, P. Schmuki, A Review of Photocatalysis using Self-organized TiO 2 Nanotubes and Other Ordered Oxide Nanostructures, Small. 8 (2012) 3073–3103. doi:10.1002/smll.201200564.

[37] M. Zlamal, J.M. Macak, P. Schmuki, J. Krýsa, Electrochemically assisted photocatalysis on self-organized TiO2 nanotubes, Electrochem. Commun. 9 (2007) 2822–2826. doi:10.1016/J.ELECOM.2007.10.002.

[38] J.M. Macak, M. Zlamal, J. Krysa, P. Schmuki, Self-Organized TiO2 Nanotube Layers as Highly Efficient Photocatalysts, Small. 3 (2007) 300–304. doi:10.1002/smll.200600426.

[39] D. Regonini, G. Chen, C. Leach, F.J. Clemens, Comparison of photoelectrochemical properties of TiO2 Nanotubes and sol-gel, Electrochim. Acta. 213 (2016) 31–36. doi:10.1016/J.ELECTACTA.2016.07.097.

[40] N.R. De Tacconi, C.R. Chenthamarakshan, G. Yogeeswaran, A. Watcharenwong, R.S. De Zoysa, N.A. Basit, K. Rajeshwar, Nanoporous TiO 2 and WO 3 Films by Anodization of Titanium and Tungsten Substrates: Influence of Process Variables on Morphology and Photoelectrochemical Response †, J. Phys. Chem. C. 110 (2006) 25347–25355. doi:10.1021/jp064527v.

[41] L. Tsui, T. Homma, G. Zangari, Photocurrent Conversion in Anodized TiO 2 Nanotube Arrays: Effect of the Water Content in Anodizing Solutions, J. Phys. Chem. C. 117 (2013) 6979–6989. doi:10.1021/jp400318n.

[42] J.M. Macák, H. Tsuchiya, A. Ghicov, P. Schmuki, Dye-sensitized anodic TiO2 nanotubes, Electrochem. Commun. 7 (2005) 1133–1137. doi:10.1016/J.ELECOM.2005.08.013.

[43] Kai Zhu, Nathan R. Neale, A. Alexander Miedaner, A.J. Frank*, Enhanced Charge-Collection Efficiencies and Light Scattering in Dye-Sensitized Solar Cells Using Oriented TiO2 Nanotubes Arrays, Nano Lett. 7 (2007) 69–74. doi:10.1021/NL062000O.

[44] S.P. Albu, A. Ghicov, S. Aldabergenova, P. Drechsel, D. LeClere, G.E. Thompson, J.M. Macak, P. Schmuki, Formation of Double-Walled TiO 2 Nanotubes and Robust Anatase Membranes, Adv. Mater. 20 (2008) 4135–4139. doi:10.1002/adma.200801189.

[45] S. Berger, S.P. Albu, F. Schmidt-Stein, H. Hildebrand, P. Schmuki, J.S. Hammond, D.F. Paul, S. Reichlmaier, The origin for tubular growth of TiO2 nanotubes: A fluoride rich layer between tube-walls, Surf. Sci. 605 (2011) L57–L60. doi:10.1016/J.SUSC.2011.06.019.

[46] N. Liu, H. Mirabolghasemi, K. Lee, S.P. Albu, A. Tighineanu, M. Altomare, P. Schmuki, Anodic TiO2 nanotubes: double walled vs. single walled, Faraday Discuss. 164 (2013) 107–116. doi:10.1039/c3fd00020f.

[47] S. Mohajernia, A. Mazare, I. Hwang, S. Gaiaschi, P. Chapon, H. Hildebrand, P. Schmuki, Depth elemental characterization of 1D self-aligned TiO2 nanotubes using calibrated radio frequency glow discharge optical emission spectroscopy (GDOES), Appl. Surf. Sci. 442 (2018) 412–416. doi:10.1016/j.apsusc.2018.02.185.

[48] A. Dronov, I. Gavrilin, E. Kirilenko, D. Dronova, S. Gavrilov, Investigation of anodic TiO2 nanotube composition with high spatial resolution AES and ToF SIMS, Appl. Surf. Sci. 434 (2018) 148–154. doi:10.1016/J.APSUSC.2017.10.132.

[49] H. Mirabolghasemi, N. Liu, K. Lee, P. Schmuki, Formation of ‘single walled’ TiO2 nanotubes with significantly enhanced electronic properties for higher efficiency dye-sensitized solar cells, Chem. Commun. 49 (2013) 2067–2069. doi:10.1039/c3cc38793c.

[50] S. So, I. Hwang, P. Schmuki, Hierarchical DSSC structures based on “single walled” TiO 2 nanotube arrays reach a back-side illumination solar light conversion efficiency of 8%, Energy Environ. Sci. 8 (2015) 849–854. doi:10.1039/C4EE03729D.

[51] S. So, F. Riboni, I. Hwang, D. Paul, J. Hammond, O. Tomanec, R. Zboril, D.R. Sadoway, P. Schmuki, The double-walled nature of TiO 2 nanotubes and formation of tube-in-tube structures – a characterization of different tube morphologies, Electrochim. Acta. 231 (2017) 721–731. doi:10.1016/j.electacta.2017.02.094.

[52] M. Motola, H. Sopha, M. Krbal, L. Hromádko, Z.O. Zmrhalová, G. Plesch, J.M. Macak, Comparison of photoelectrochemical performance of anodic single- and double-walled TiO<inf>2</inf>nanotube layers, Electrochem. Commun. 97 (2018). doi:10.1016/j.elecom.2018.09.015.

[53] X. Lu, G. Wang, T. Zhai, M. Yu, J. Gan, Y. Tong, Y. Li, Hydrogenated TiO_2 Nanotube Arrays for Supercapacitors, Nano Lett. 12 (2012) 1690–1696. doi:10.1021/nl300173j.

[54] Z. Lu, C.-T. Yip, L. Wang, H. Huang, L. Zhou, Hydrogenated TiO_2 Nanotube Arrays as High-Rate Anodes for Lithium-Ion Microbatteries, Chempluschem. 77 (2012) 991–1000. doi:10.1002/cplu.201200104.

[55] S. Zhou, S. Liu, K. Su, K. Jia, Facile synthesis of Ti3+ self-doped and sulfur-doped TiO2 nanotube arrays with enhanced visible-light photoelectrochemical performance, J. Alloys Compd. 804 (2019) 10–17. doi:10.1016/J.JALLCOM.2019.06.294.

[56] J. Dong, J. Han, Y. Liu, A. Nakajima, S. Matsushita, S. Wei, W. Gao, Defective Black TiO_2 Synthesized via Anodization for Visible-Light Photocatalysis, ACS Appl. Mater. Interfaces. 6 (2014) 1385–1388. doi:10.1021/am405549p.

[57] M. Krbal, H. Sopha, D. Pohl, L. Benes, C. Damm, B. Rellinghaus, J. Kupčík, P. Bezdička, J. Šubrt, J.M. Macak, Self-organized TiO2 nanotubes grown on Ti substrates with different crystallographic preferential orientations: Local structure of TiO2 nanotubes vs. photo-electrochemical response, Electrochim. Acta. 264 (2018) 393–399.

doi:10.1016/J.ELECTACTA.2018.01.113.

[58] R. Beranek, H. Tsuchiya, T. Sugishima, J.M. Macak, L. Taveira, S. Fujimoto, H. Kisch, P. Schmuki, Enhancement and limits of the photoelectrochemical response from anodic TiO2 nanotubes, Appl. Phys. Lett. 87 (2005) 243114. doi:10.1063/1.2140085.

[59] A.I. Kuznetsov, O. Kameneva, A. Alexandrov, N. Bityurin, A. K. Chhor, † A. Kanaev*, Chemical Activity of Photoinduced Ti3+ Centers in Titanium Oxide Gels, J. Phys. Chem. B. 110 (2006) 435–441. doi:10.1021/JP0559581.

[60] Z.Q. Bai, Z.W. Liu, A broadband photodetector based on Rhodamine B-sensitized ZnO nanowires film, Sci. Rep. 7 (2017). doi:10.1038/s41598-017-11154-8.

[61] A. Knowles, A Mechanism for the methylene blue sensitized oxidation of nucleotides, Photochem. Photobiol. 13 (1971) 473–487. doi:10.1111/j.1751-1097.1971.tb06142.x.

[62] X. Cheng, Q. Cheng, B. Li, X. Deng, J. Li, P. Wang, B. Zhang, H. Liu, X. Wang, One-step construction of N/Ti3+ codoped TiO2 nanotubes photoelectrode with high photoelectrochemical and photoelectrocatalytic performance, Electrochim. Acta. 186 (2015) 442–448. doi:10.1016/j.electacta.2015.11.005.

[63] Y.J. Hwang, S. Yang, H. Lee, Surface analysis of N-doped TiO2 nanorods and their enhanced photocatalytic oxidation activity, Appl. Catal. B Environ. 204 (2017) 209–215. doi:10.1016/j.apcatb.2016.11.038.

[64] M.T. Nguyen-Le, B.K. Lee, Effective photodegradation of dyes using in-situ N-Ti3+ co-doped porous titanate-TiO2 rod-like heterojunctions, Catal. Today. 297 (2017) 228–236. doi:10.1016/j.cattod.2017.03.036.

[65] K. Li, S. Gao, Q. Wang, H. Xu, Z. Wang, B. Huang, Y. Dai, J. Lu, In-situ-reduced synthesis of Ti^{3+} self-doped TiO<inf>2</inf>/g-C<inf>3</inf>N<inf>4</inf>

heterojunctions with high photocatalytic performance under LED light irradiation, ACS Appl. Mater. Interfaces. 7 (2015) 9023–9030. doi:10.1021/am508505n.

[66] M. Li, Z. Xing, J. Jiang, Z. Li, J. Yin, J. Kuang, S. Tan, Q. Zhu, W. Zhou, Surface plasmon resonance-enhanced visible-light-driven photocatalysis by Ag nanoparticles decorated S-TiO2−x nanorods, J. Taiwan Inst. Chem. Eng. 82 (2018) 198–204. doi:10.1016/j.jtice.2017.11.023.

[67] Z. Xiu, M. Guo, T. Zhao, K. Pan, Z. Xing, Z. Li, W. Zhou, Recent advances in Ti3+ self-doped nanostructured TiO2 visible light photocatalysts for environmental and energy applications, Chem. Eng. J. (2019) 123011. doi:10.1016/j.cej.2019.123011.

[68] J. Yan, G. Wu, N. Guan, L. Li, Z. Li, X. Cao, Understanding the effect of surface/bulk defects on the photocatalytic activity of TiO2: Anatase versus rutile, Phys. Chem. Chem. Phys. 15 (2013) 10978–10988. doi:10.1039/c3cp50927c.